Chemical Engineering Journal 493 (2024) 152711

Contents lists available at ScienceDirect

Chemical Engineering Journal

journal homepage: www.elsevier.com/locate/cej

Sprayable hydrogel with optical mRNA nanosensors for Real-Time monitoring and healing of diabetic wounds

Daun Jeong [a,d,1], Se Youn Jang [b,1], Soonjong Roh [b,h], Ji Hye Choi [a,d], I Ji Seo [c], Jin Hyuck Lee [d], Jihoon Kim [c], Ilkeun Kwon [e], Youngmee Jung [b,f], Jangsun Hwang [a,d,*], Woo Young Jang [a,d,*], Jin Yoo [b,g,**]

[a] Department of Orthopedic Surgery, Korea University College of Medicine, Seoul 02841, Republic of Korea
[b] Biomaterials Research Center, Biomedical Research Institute, Korea Institute of Science and Technology (KIST), Seoul 02792, Republic of Korea
[c] Advanced Biomolecular Recognition Center, Biomedical Research Institute, Korea Institute of Science and Technology (KIST), Seoul 02792, Republic of Korea
[d] Institute of Nanobiomarker-Based Medicine, Korea University, Seoul 02841, Republic of Korea
[e] Department of Dental Materials, School of Dentistry, Kyunghee University, Seoul 02447, Republic of Korea
[f] School of Electrical Electronic Engineering, YU-KIST Institute, Yonsei University, Seoul 03722, Republic of Korea
[g] Division of Bio-Medical Science and Technology, KIST school, Korea University of Science and Technology (UST), Seoul 02792, Republic of Korea
[h] Department of Applied Bioengineering, Graduate School of Convergence Science and Technology, Seoul National University, Seoul 08826, Republic of Korea

ARTICLE INFO

Keywords:
Sprayable hydrogels
Nanosensor
Wound healing
Diabetic wound
Antimicrobial peptides

ABSTRACT

Sprayable hydrogels offer a promising approach for treating diabetic wounds. They possess the capability to conform to irregular surfaces, create a moist environment that supports the growth of new tissue, and offer protection against infections. Yet, applying previously reported sprayable hydrogels has proven to be challenging, often necessitating the use of specialized equipment or the simultaneous injection of multiple components. In this study, we develop a user-friendly therapeutic hydrogel that can be applied using a general spray bottle. This hydrogel is formulated using the bioactive agent, LL37, which is known for its antimicrobial properties and ability to enhance angiogenesis. Additionally, optical mRNA nanosensors, NanoFlares, were incorporated into the hydrogel to measure the expression of proliferation and inflammation biomarkers, providing precise molecular-based parameters for evaluating diabetic wound status. The efficacy of LL37- and NF-incorporated hydrogels in promoting *in vivo* wound healing in normal and diabetic mice is evaluated, and a Wound Healing Index (WHI) is presented to assist medical professionals in making informed decisions about wound care and treatment. Overall, our study demonstrates the potential of sprayable hydrogels for promoting diabetic wound healing and monitoring the diabetic wound status, which could have significant potential for future clinical applications.

1. Introduction

Hydrogels have been traditionally used as wound dressings because of their high water content and excellent physical properties [1–3]. Sprayable hydrogels (SHs) offer numerous advantages over traditional hydrogels, which are typically used as preformed sheets or gels [4]. One key benefit is their ability to be easily sprayed onto irregular surfaces, thereby forming thin and transparent films that provide better coverage and conformability to the target area. Furthermore, they provide a moist environment that supports tissue formation and protects wounds from infection [5]. Additionally, SH can be engineered to possess a wide range of physical, chemical, and biological properties such as stiffness, porosity, bioactivity, and biodegradability, which can be tailored to meet specific tissue requirements [6,7]. For effective spray administration, materials must exhibit shear-thinning properties. This allows the material to be delivered in a sol-like state and then transition in situ to a

* Corresponding authors at: Department of Orthopedic Surgery, Korea University College of Medicine, Seoul 02841, Republic of Korea.
** Corresponding author at: Biomaterials Research Center, Biomedical Research Institute, Korea Institute of Science and Technology (KIST), Seoul 02792, Republic of Korea.
E-mail addresses: isnickawesome@gmail.com (J. Hwang), opmanse@korea.ac.kr (W.Y. Jang), jyoo@kist.re.kr (J. Yoo).
[1] These authors contributed equally to this work.

https://doi.org/10.1016/j.cej.2024.152711
Received 19 January 2024; Received in revised form 29 April 2024; Accepted 30 May 2024
Available online 31 May 2024

gel-like state through crosslinking. Therefore, the material design and mechanical properties are critical for the development of SH for biomedical applications. In this context, laponite hydrogels have garnered attention owing to several advantages over conventional hydrogels, such as high transparency, shear-thinning behavior, and tunable mechanical properties [8,9].

Wound healing is a complex process that entails the spatial and temporal synchronization of several cell types with diverse functions during the stages of hemostasis, inflammation, growth, re-epithelialization, and remodeling [10–12]. Wounds in which the healing process does not occur in a normal, orderly, or timely manner are referred to as chronic wounds [13–15]. The diabetic wound, is a type of chronic wound that often occurs on the feet, legs, or toes of people with diabetes mellitus (DM). One of the major factors is hyperglycemia, which hinders proper inflammation, proliferation, and re-epithelialization, increases the risk of infection leading to impaired wound healing in patients with DM [16–18]. About 15 % of patients with diabetes are at risk of developing diabetic wounds, which can lead to amputation of lower extremities if the diabetic wounds are not properly detected and treated [19]. Moreover, diabetic wounds are more susceptible to infection than nondiabetic wounds [20,21] and they can be avoided through timely and efficient medical intervention [22]. Therefore, proper management of diabetic wounds is important to maximize the therapeutic effect. From this viewpoint, wound-healing monitoring systems are valuable tools for managing chronic wounds and improving patient outcomes. Several methods used to determine the state of a wound include macroscopic observations (e.g., inspection, photography, or regular video image capture) [23] as well as examination of biological parameters (e.g., pH, temperature, or oxygen levels) [24–26]. However, the examination of molecular biomarkers, including proteins, DNA, and RNA, is the most precise and concrete parameter for evaluating wound status [27].

SHs have shown numerous advantages in the field of wound healing as dressings for chronic wounds, including nonhealing diabetic wounds, owing to their superior biochemical and mechanical properties [6,28,29]. However, previously reported SHs require the simultaneous injection of two or more components for in situ chemical reactions [30,31], making the application process challenging. Moreover, physical crosslinking of hydrogels, such as self-assembly-triggered gelation, necessitates the use of infusion pumps [9], atomization devices [32], and nebulizers for the spraying process. Therefore, there is a need to develop a multifunctional material that is both user-friendly and capable of effectively promoting diabetic wound healing.

In this study, we developed a multifunctional therapeutic SH that can monitor the condition of diabetic wounds in real time, promote wound healing, and can be applied using a general spray bottle without the need for an atomizer [32] or other devices. To monitor the diabetic wound healing status at the molecular level, we applied several diabetic wound healing-related mRNA biomarkers that were previously selected in our previous study [27] and designed optical mRNA nanosensors (i.e., NanoFlare (NF)) capable of detecting and quantifying them. In addition, LL37, an antimicrobial agent that can prevent infection and promote regeneration [33], was applied to increase the healing efficiency of diabetic wounds, because these wounds have poor regeneration efficiency and are vulnerable to infection [20]. LL37, a cathelicidin antimicrobial peptide of human origin, not only reduces susceptibility to skin infection, but also regulates immune activity, angiogenesis and cell proliferation [34,35]. We hypothesized that the fabricated multifunctional SH would increase the diabetic wound healing efficiency. The optimal properties of the SH and the efficacy of the NFs and LL37 were evaluated in vitro, and the diabetic wound-healing efficiency of the fabricated multifunctional SH was confirmed *in vivo*.

2. Results and discussion

Simultaneous Wound Healing and Monitoring System High-level diagnostic and detection methods are necessary to monitor the progression of diabetic ulcers, and effective, non-invasive, and simple treatments are essential. In this context, we developed a SH that enables simultaneous treatment and monitoring of the wound site.

The hydrogel matrix was composed of laponite and poly(acrylic acid) (PAA). Laponite is a synthetic clay that forms hydrogels when dispersed in water. Laponite exhibits an anisotropic charge distribution, with negative charges on the faces and positive charges on the edges. The high viscosity of laponite solutions has been attributed to a gelation process caused by face-edge attractions, known as the house of cards' structure, in which clay particles self-assemble into a crosslinked network and trap water molecules. PAA was used as a crosslinker for clay nanoparticles and as a skin-adhesive material. PAA is known for its bioadhesive properties, as its carboxyl groups can contribute to soft tissue adhesion through hydrogen-bonding interactions [36]. Moreover, the negatively charged groups of PAA interacted with laponite nanodiscs, resulting in a change in the self-assembly of the house-of-the-card structure by forming a hydrogel matrix.

The biocompatible hydrogel was incorporated with NFs and the antimicrobial peptide, LL37 (Scheme 1). NFs facilitate real-time monitoring of the wound healing stages of inflammation, proliferation, and remodeling using portable fluorescent imaging devices by detecting the target mRNA with fluorescence. NFs, which are based on gold nanoparticles (GNPs), are fabricated by attaching a complementary sequence (Recognition; R) that recognizes the desired mRNA sequence (Target; T) and a dye conjugated short single-stranded DNA (ssDNA) sequence (Flare; F) on Recognition. In a previous study, the target signal was identified using quantitative fluorescence signals from an *in vivo* imaging system (IVIS) [27]. Therefore, portable *in vivo* fluorescence imaging devices have the potential to be used. Collectively, NFs and LL37 were successfully encapsulated in the SH, providing an easy-to-use hydrogel for monitoring and treating diabetic wounds.

Preparation of a Sprayable Hydrogel To obtain a transparent solution, laponite was dispersed in deionized water with vigorous magnetic stirring. The laponite solutions were prepared at 2 % w/v of nanodiscs, resulting in a viscous solution after aging for one day. However, the aged 2 % w/v solution remained liquid and flowed to the bottom of the vials upon inversion [37]. The SH was prepared by mixing the laponite dispersion and a PAA solution with a higher molecular weight (>100 kDa) and manually swirling the gel within 30 s. Interestingly, when the molecular weight of PAA was low (i.e., 5 kDa), the mixture could not form a hydrogel, and the viscosity of the solution decreased, as previously reported [38]. The introduction of short-chain PAA into the system is expected to result in adsorption onto the positively charged edges of laponite sheets through electrostatic interactions, reducing the electrostatic interactions between the nanodiscs themselves and accelerating the dispersion of the laponite sheets [39]. Conversely, when long chains of PAA (i.e., 100 kDa, 240 kDa) were introduced into the system, the viscous solution became a hydrogel formulation, as shown in Fig. 1A. Anionic PAA enables the exfoliation and dispersion of laponite by mutual repulsion resulting from the site-specific wrapping of positively charged edge parts [40,41]. Thus, the long chains of PAA act as crosslinkers, leading to hydrogel formation immediately after simple mixing.

First, because the salt concentration is known to have a significant effect on the self-assembly of laponite sheets, the amount of PBS added was carefully controlled. PBS acts as an ionic crosslinker, resulting in a laponite hydrogel [42]. However, when an excess amount of salt was introduced into the laponite dispersion, laponite coagulation occurred. The dispersion, aggregation, and coagulation of laponite could be altered by adjusting the ionic strength of the solution [42]. We investigated the effect of PBS on the rheological behavior of SHs. Oscillatory measurements indicate that both the storage modulus (G') and loss modulus (G'') of SHs increased with the addition of PBS (Fig. 1B). We confirmed that an appropriate amount of 10X PBS buffer led to an increase in mechanical strength; however, an excess amount of salt

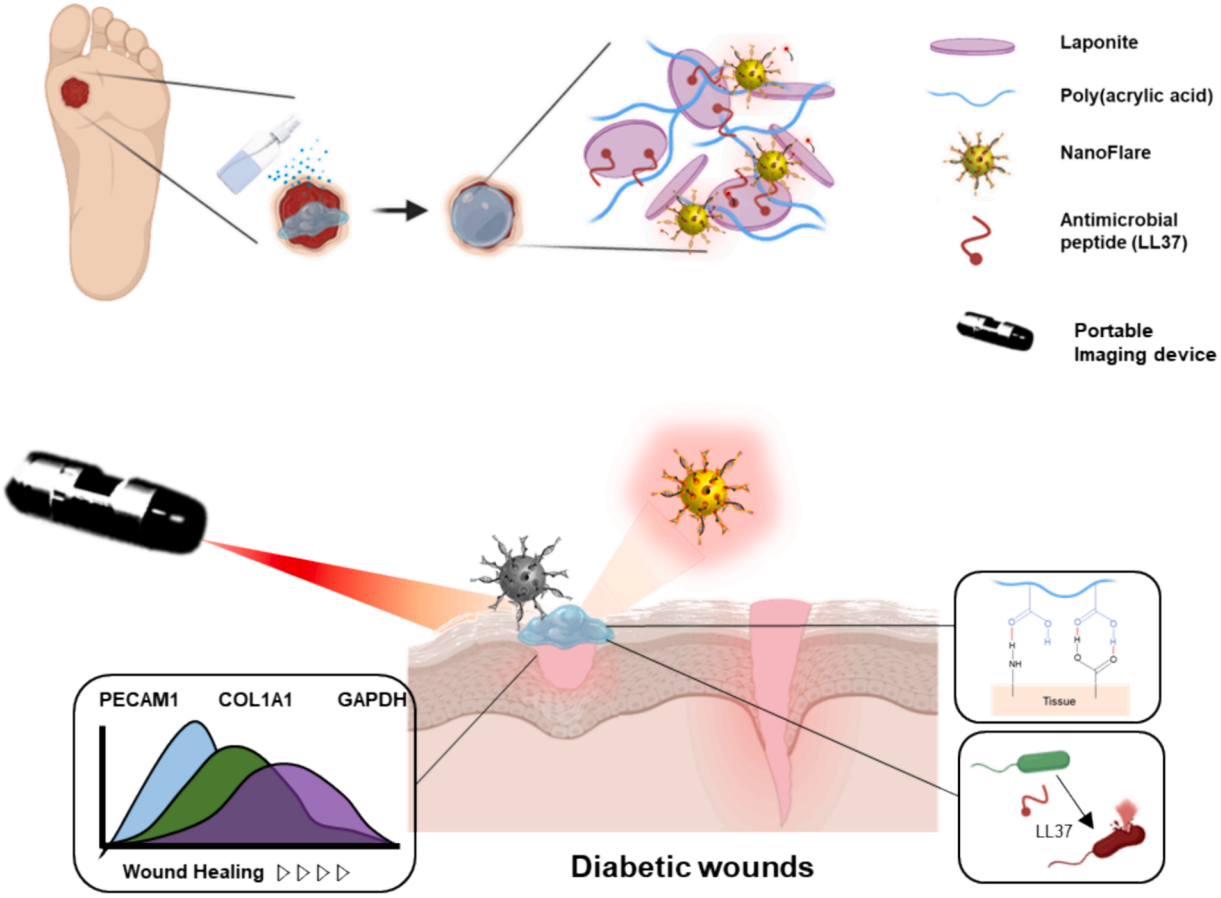

Scheme 1. Schematic illustration of a sprayable hydrogel (SH) with NanoFlares and antimicrobial peptides (LL37) for monitoring diabetic wounds and promoting wound healing.

induced the coagulation of laponite, resulting in a decrease in mechanical strength and transmittance in the visible wavelength range (Fig. 1B and Fig. S1). Taken altogether, we found that 25 μL of 10X PBS buffer was the optimal amount for 2 mL of laponite solution to increase the mechanical strength of SH, whereas 50 μL of PBS was an excess amount.

Next, we investigated the effect of molecular weight (M_w) of the polymer on the composite hydrogel. We studied the rheological properties and sprayability of blended hydrogels composed of PAA and nanoclay and the effects of two M_w values, 100 kDa and 240 kDa, on them. Our findings reveal that the use of PAAs with a higher M_w results in a higher mechanical strength of the blended hydrogels, which is consistent with previous studies [43,44]. Step-strain measurements were conducted to verify the reversible gel-sol transition of the SHs. We subjected the SHs to repeated cycles of 3 min low-magnitude strain of 0.5 % and 2 min high-magnitude strain of 500 % oscillations at 6.3 rad/s to assess deformation and recovery of SHs. After applying alternating low and high strains, we monitored the moduli of the SHs during strain changes. As shown in Fig. 1C, the gels underwent gel-sol transition and behaved as liquids upon increasing the oscillatory strain from 0.5 % to 500 %. In contrast, the SHs rapidly underwent sol–gel transition and recovered back to their initial moduli immediately upon lowering the strain from 500 % to 0.5 % [40]. The gel-sol transition was reversible, and the gels were capable of self-healing to their original state without compromising their mechanical fidelity, even after multiple shear-thinning cycles. These data indicate the robust reversibility of the mechanical properties of SHs.

While SHs composed of 240 kDa PAA exhibit shear-thinning and better mechanical properties, as shown in Fig. S2A, the sprayability of SHs with 100 kDa PAA was better because of their ability to spread well and cover a larger area, as demonstrated in Fig. 1D. The SHs prepared in this study were easily injected through a 22-gauge needle and immediately reformed into a solid gel after injection. SHs with better mechanical properties facilitate the immediate reformation of a steady gel after injection, resulting in a higher resolution and retention of the original shape. However, when considering the distribution and spread area following spraying, the optimized conditions were SHs with 100 k PAA and PBS, as they facilitate the coverage of wound areas during wound healing. The distribution of the SHs was captured after spraying at a distance of 20 cm. Furthermore, the self-healing property of the optimized SH was confirmed by injecting it into fresh wounds of Sprague–Dawley (SD) rats with an incision in the dorsum panniculus carnosus [5]. After subjecting the SH to a series of cuts, stretching, squeezing, and other external forces that could alter its shape (Fig. 1E), the SH remained adhered to the wounds and was able to restore its original shape while resisting various external forces applied to the hydrogel-covered wounds. This further validates the excellent properties of the hydrogel as a dressing for treating diabetic skin wounds.

Finally, we examined the effect of varying the amount of the PAA solution introduced into the system. When insufficient PAA was added, the sol–gel transition did not occur, resulting in a still-flowing viscous solution. Surprisingly, excess addition of PAA led to a decrease in the mechanical strength of the hydrogel (Fig. S2B). Although PAA chains are expected to bridge clay particles, an excess of PAA chains can aggregate and fail to act as crosslinkers, thereby degrading the mechanical properties of the blended hydrogels. In conclusion, the amounts of PAA, PBS, and laponite introduced into SH were optimized by considering the mechanical properties and sprayability, as discussed above.

Design, Synthesis, Properties, and Optimization of NFs In a previous study, we identified the target genes associated with the

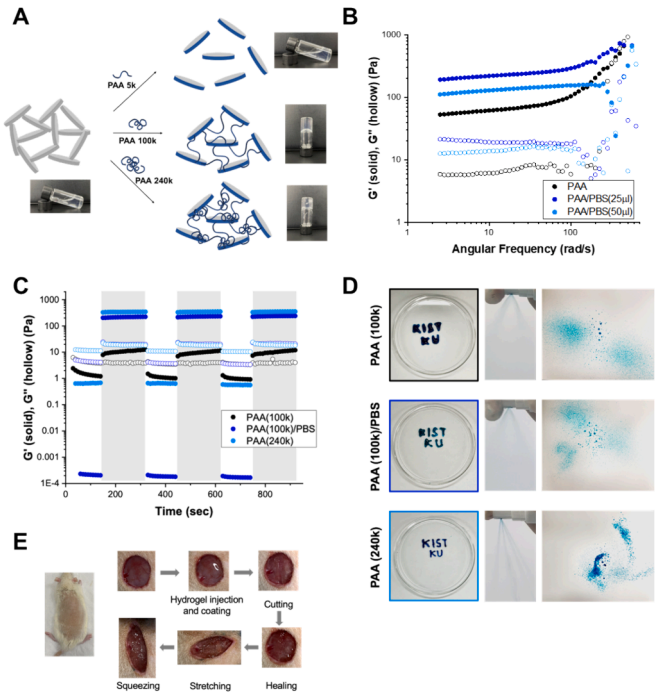

Fig. 1. Preparation of a sprayable hydrogel. (A) Schematic fabrication of the hydrogel composed of laponite and polyacrylic acid (PAA) with different molecular weights. (B) The storage and loss moduli of the hydrogel with varying phosphate-buffered saline (PBS) concentrations as a function of the frequency, using an oscillatory strain of 1 %. (C) The deformation and recovery of hydrogels. Gels evolved over time from repeated cycles of 3 min of low 0.5 % strain and 2 min of high 500 % strain oscillations at 6.3 rad/s. (D) The feasibility of injecting and spraying hydrogels, along with the corresponding distribution of sprayed hydrogel formulations. (E) Sprague–Dawley (SD) rats with full-thickness wounds, followed by injection of the hydrogels.

inflammatory and proliferative stages of wound healing.[27] Based on this, we synthesized NFs targeting these specific mRNA biomarkers as follows; platelet and endothelial cell adhesion molecule 1 (*PECAM1*), and collagen type I α 1 (*COL1A1*) mRNAs were selected as target biomarkers for immune cells (inflammation stage), and fibroblasts (collagen formation and proliferation stage), respectively (Fig. S3A-G) [27,45,46]. Additionally, the glyceraldehyde-3-phosphate dehydrogenase (*GAPDH*) reference gene was used to serve as an endogenous control signal as well as for cellular quantification. The average size of NFs was 17 ± 3 nm and the Zeta potential decreased from −20 mV to –33 mV when NFs were synthesized (Fig. S4A and B). As shown in Fig. S4C, all the NFs showed excellent sensitivity and selectivity for their respective target sequences. For example, when PECAM1-NF encountered its target mRNA sequence, the fluorescence intensity increased over 30-fold. In addition, COL1A1-NF, PECAM1-NF, and GAPDH-NF showed better sensitivity with good correlation with target reactivity between 0.001 and 10 μM (Fig. S4D and E, R2 = 0.96, 0.911, and 0.988, respectively).

Growth Factor Screening using NFs to Monitor Target Genes To evaluate dynamic performance of the NFs during wound healing stages, the stimulating effect of five exogenous growth factors (i.e., tumor necrosis factor- α [TNF-α], transforming growth factor beta 1 [TGF-β1], interleukin-6 [IL-6], platelet-derived growth factor [PDGF], and fibroblast growth factor 2 [FGF-2]) was observed in normal and high glucose conditions (25 mM). All data are presented as the mean fold change compared to the untreated (no-treatment) data for each group. Fig. 2A, D, and Fig. S5 show the expression levels of *COL1A1* mRNA in response to growth factors in normal human dermal fibroblasts (NDFs) under normal and high glucose conditions. In the normal condition, quantitative polymerase chain reaction (qPCR) analyses showed that there was no significant change in *COL1A1* mRNA expression following the treatment with TNF-α (0.95-fold), IL-6 (1.0-fold) and PDGF (0.91-fold). However, TGF-β1 (4.1-fold) dramatically increased *COL1A1* mRNA expression, whereas FGF2 (0.57-fold) expression was downregulated (Fig. 2A, bars). We observed no changes in the COL1A1-NF signals under normal conditions after treatment with IL-6 (0.99-fold) and FGF-2 (0.97-fold). However, COL1A1-NF signal decreased in the samples treated with TNF-α (0.82-fold) and increased in TGF-β1 (1.19-fold) and PDGF (1.11-fold) (Fig. 2A, line). Hence, the results of the qPCR and NF analyses were highly concordant. In contrast, in high glucose conditions, qPCR analyses showed an increase in *COL1A1* mRNA expression following treatment with exogenous TGF-β1 (3.75-fold), IL-6 (3.41-fold), and PDGF (1.21-fold). No significant changes were observed following FGF-2 treatment (0.99-fold increase). However, TNF-α (0.41-fold) dramatically decreased *COL1A1* mRNA expression in the high glucose condition (Fig. 2D, bars). Furthermore, we observed that the COL1A1-NF fluorescence signal increased in response to exogenous TGF-β1 (1.12-fold), IL-6 (1.11-fold), PDGF (1.09-fold) and FGF-2 (1.14-fold) treatment, and decreased in response to TNF-α (0.93-fold) treatment, in the high glucose condition (Fig. 2D, line). Therefore, the qPCR and NF results were concordant.

As shown in Fig. 2B, E, and Fig. S6, the expression of *PECAM1* mRNA in THP-1 cells was analyzed under normal (Fig. S6A) and high glucose conditions (25 mM, Fig. S6B). qPCR analyses showed that the expression level of *PECAM1* mRNA was increased in all samples; TNF-α (1.8-fold), TGF-β1 (8.75-fold), IL-6 (1.49-fold), PDGF (2.58-fold), and FGF-2 (1.24-fold) (Fig. 2B, bars). Additionally, we observed the PECAM1-NF signal increased in all sample groups; TNF-α (1.27-fold), TGF-β1 (2.21-fold), IL-6 (1.61-fold), PDGF (1.37-fold), and FGF-2 (1.39-fold) (Fig. 2B, line). In contrast, in the high glucose condition, expression of *PECAM1* mRNA analyzed by qPCR showed that the NF signal increased following the treatment with TGF-β1 (2.6-fold), PDGF (1.34-fold), and FGF-2 (1.9-fold), and decreased in samples treated with TNF-α (0.4-fold) and IL-6 (0.85-fold) (Fig. 2E, bars). We observed that the PECAM1-NF signal slightly increased following the treatment with TGF-β1 (1.08-fold) and FGF-2 (1.11-fold), and dramatically decreased in TNF-α (0.79-fold) and IL-6 (0.59-fold)-treated samples (Fig. 2E, line). Therefore, the expression levels from qPCR and the signal analysis of the NFs were highly correlated.

Alternatively activated (M2) macrophages are key components of wound healing and are known to exert anti-inflammatory effects [47–49]. To monitor M2 macrophage [49] activity during the inflammation stage under diabetic conditions, THP-1 cells were polarized into M2 macrophages using exogenous cytokines (interleukin-4 [IL-4] and interleukin-10 [IL-10]) [50,51]. Laser scanning confocal microscopy (LSCM) images of cytokine-polarized M2 macrophages are presented in Fig. S7A and B, showing the expression level of Cluster of Differentiation 206 (CD206), a marker for M2 macrophages [52]. Compared to the no-treatment group, CD206 expression increased (2.7-fold) in cells treated with IL-4 and IL-10 under normal conditions. In contrast, in the high glucose (25 mM) condition, CD206 expression was increased (1.83-fold), but was relatively lower than that in the normal condition. These results are consistent with those of previous studies that showed a relative reduction in M2 macrophage polarization under hyperglycemic conditions [53]. Additionally, mouse *PECAM1* (m*PECAM1*) mRNA expression was monitored with mPECAM1-NF in a mouse macrophage cell line (RAW 264.7; Fig. S7C and D). LSCM images showed that the fluorescence signal level of mPECAM-NF increased significantly by exogenous IL-6 (40 %), TNF-α (10 %), and lipopolysaccharide (LPS) (15 %) compared to the no-treatment group. As shown in Fig. 2C, F, and Fig. S8, we measured the expression level of *PECAM1* mRNA in cytokine-polarized M2 macrophages using qPCR and NF under normal (Fig. S8A) and high-glucose (25 mM, Fig. S8B) conditions treated with five exogenous growth factors. qPCR analyses showed that expression of *PECAM1* mRNA in the normal condition increased following the treatment with TGF-β1 (5.98-fold), IL-6 (1.79-fold), and PDGF (1.41-fold) and

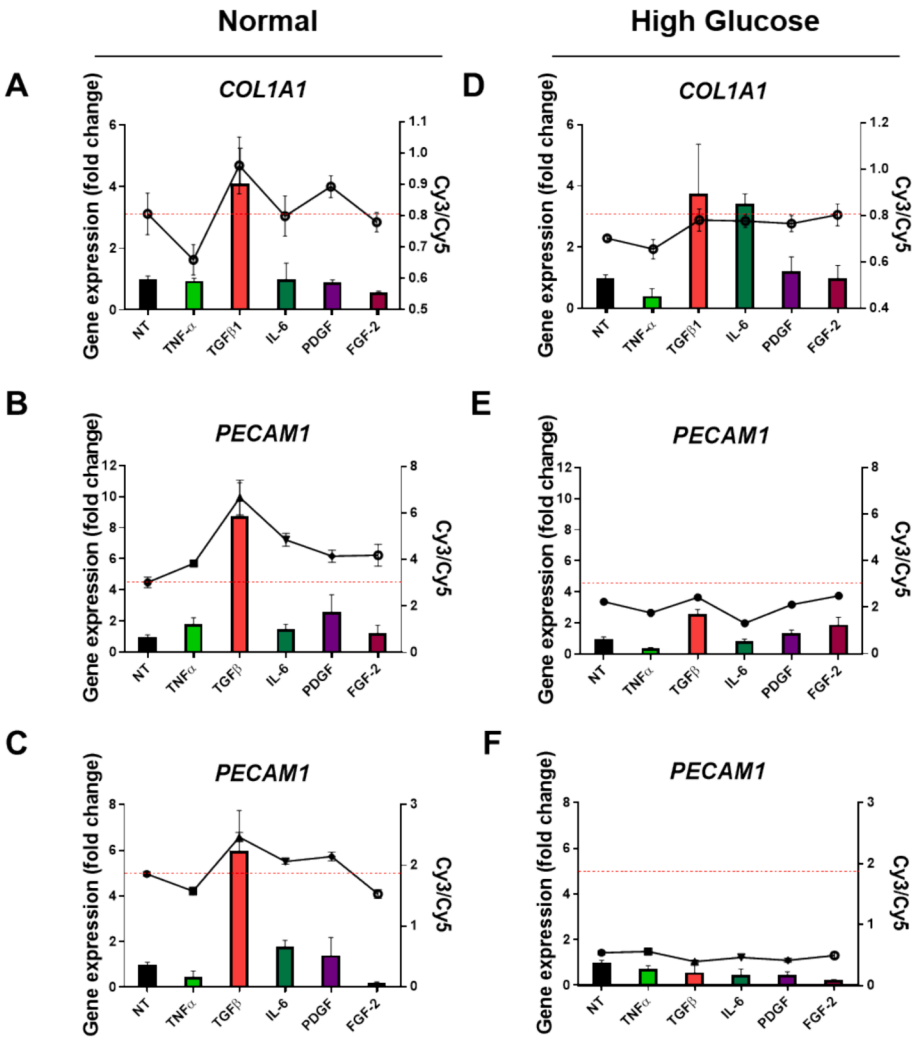

Fig. 2. Evaluation of target genes by NanoFlares (NFs) and quantitative polymerase chain reaction (qPCR). (A) Collagen type I α 1 (*COL1A1*) mRNA expression in normal human dermal fibroblasts (NDFs) in the normal condition. (B) Platelet and endothelial cell adhesion molecule 1 (*PECAM1*) mRNA expression in THP-1 cells in the normal condition. (C) *PECAM1* mRNA expression in cytokine-polarized M2 macrophages in the normal condition. (D) *COL1A1* mRNA expression in NDFs in the high glucose condition. (E) *PECAM1* mRNA expression in THP-1 cells in the high glucose condition. (F) *PECAM1* mRNA expression in cytokine-polarized M2 macrophages in the high glucose condition (NT = No-treatment, *GAPDH* normalization, line = fluorescence signal from each NF, bars = fold change analyzed with qPCR, red horizontal dot lines = baseline fluorescence signal of each NF, n = 3, cell counts = 100, glucose = 25 mM, TNF-α = 40 ng/mL, TGFβ1 = 40 ng/mL, IL-6 = 40 ng/mL, PDGF = 20 ng/mL, FGF-2 = 40 ng/mL, M2 polarization = 40 ng/mL of IL-4 and IL-10 for 7 days).

decreased following the treatment with TNF-α (0.45-fold) and FGF-2 (0.19-fold) (Fig. 2C, bars). PECAM1-NF signal increased following the treatment with TGF-β1 (1.33-fold), IL-6 (1.11-fold), and PDGF (1.15-fold) and decreased following the treatment with TNF-α (0.85-fold) and FGF-2 (0.82-fold) (Fig. 2C, line). In the high glucose condition, *PECAM1* mRNA expression analyzed by qPCR decreased in all groups: TNF-α (0.74-fold), TGF-β1 (0.56-fold), IL-6 (0.47-fold), PDGF (0.47-fold), and FGF-2 (0.24-fold) (Fig. 2F, bars). *PECAM1* mRNA expression analyzed by PECAM1-NF in cytokine-polarized M2 macrophages decreased with TGF-β1 (0.73-fold), IL-6 (0.86-fold), PDGF (0.77-fold), and FGF-2 (0.91-fold) treatment. There was no significant change of the PECAM1-NF signal with TNF-α (1.03-fold) treatment (Fig. 2F, line). Overall, the baseline NF signals decreased under high-glucose conditions compared to those under normal conditions (red horizontal dotted lines in Fig. 2).

Incorporation of LL37 and NFs into Sprayable Hydrogel To create a SH that can enhance wound healing and facilitate monitoring, we formulated a hydrogel containing NFs and antimicrobial peptide LL37. A dual-function hydrogel was prepared by mixing LL37 and NFs with the previously prepared SH. LL37 and NFs were easily incorporated into the SH by simple stirring, which was attributed to the shear-thinning properties of SH. This allowed for easy creation of the complex hydrogel.

The rheological behavior of the complex hydrogel was investigated and compared with that of the bare SH. All hydrogels in the oscillatory measurements showed that the storage modulus (G') dominated the loss modulus (G'') across the entire frequency range applied, demonstrating the gel-like behavior of the hydrogels (Fig. 3A). Although the physical properties of the hydrogel containing only NF were similar to those of the SH, they decreased slightly in the hydrogel containing both NF and LL37. The addition of LL37 disrupted the intermolecular interactions between laponite and PAA, resulting in a lower network strength. The mechanical strength was slightly reduced when LL37 was included. However, the formation of the hydrogel was well-maintained and did not significantly affect its sprayability (Fig. S9A). Because NFs are nanosensors for the intracellular detection of mRNA, it is necessary for cells to take up NFs through endocytosis [27]. Therefore, we verified that the NFs were released from the hydrogel by quantifying their release profile from the complex hydrogel (Fig. S9B). Additionally, the release profile of LL37 from the hydrogel was also assessed, which confirmed a sustained release of the peptide as depicted in Fig. S9C.

To evaluate the deformation and recovery of the composite hydrogel,

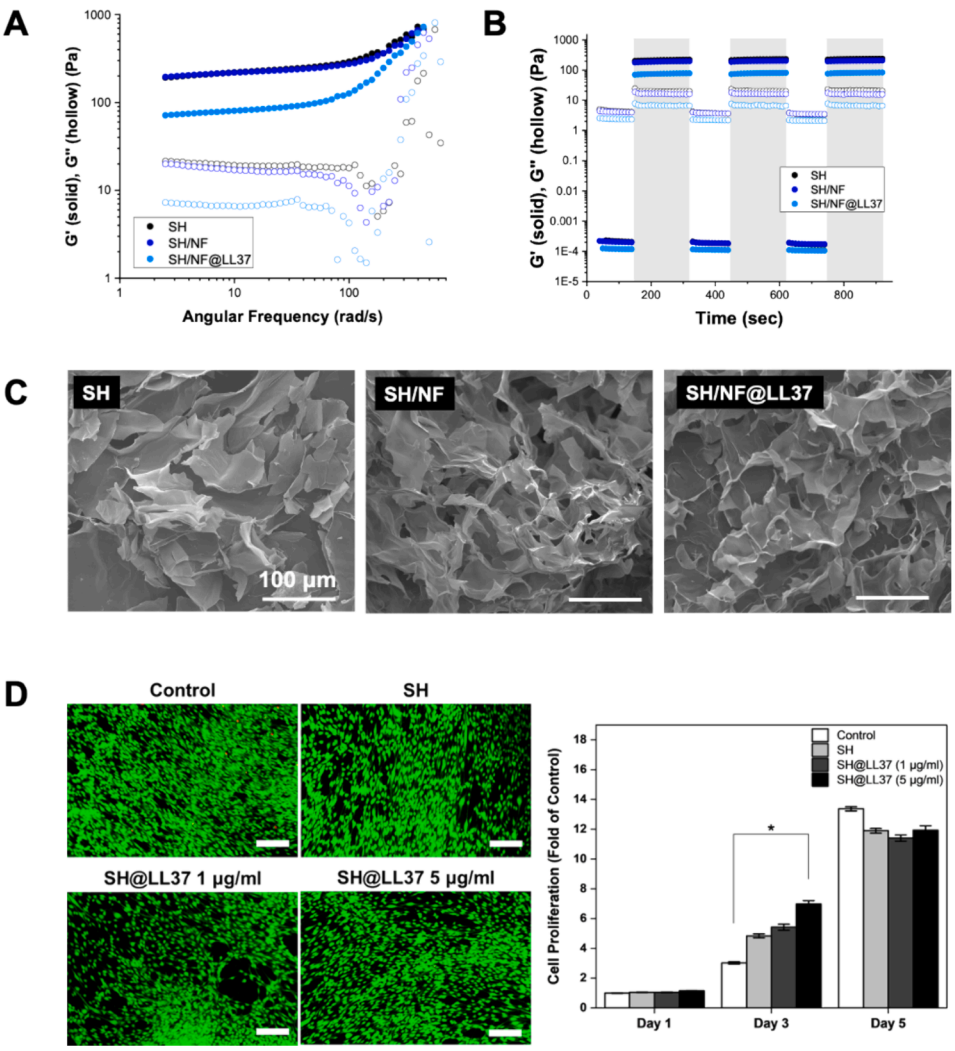

Fig. 3. Characterization of LL37 and NanoFlare (NF)-incorporated sprayable hydrogel. (A) The storage and loss moduli of the bare sprayable hydrogel (SH) and NF, and LL37-incorporated SH (SH/NF@LL37) as a function of the frequency, using an oscillatory strain of 1 %. (B) The deformation and recovery of hydrogels incorporated with NF and LL37. Gels evolved over time from repeated cycles of 3 min of low 0.5 % strain and 2 min of high 500 % strain oscillations at 6.3 rad/s. (C) Scanning electron microscope (SEM) images of the lyophilized hydrogels. (D) Quantification of cell survival and proliferation through CCK-8 analysis of NDF cells cultured for 1, 3, and 5 days in the control and LL37 containing hydrogel groups and Live/Dead staining images of NDF cells on day 5. Relative cell proliferation on days 3 and 5 was normalized based on the proliferation of cells cultured for 1 day. Surviving cells are stained green, and dead cells are stained red. Scale bar = 200 μm. $*p < 0.05$.

a continuous variation deformation between 1 % and 500 % was performed at the same strain (6.3 rad/s). Similar to previous results, although the physical properties decreased slightly in the case of the hydrogel containing LL37, the G' and G'' values of all three hydrogels were maintained even after destruction and reformation, indicating that all three hydrogels had self-healing properties (Fig. 3B). We observed scanning electron microscope (SEM) images of each hydrogel, and it was confirmed that all three hydrogels formed a matrix with a porous structure. The integration of NF and LL37 did not affect the hydrogel structure (Fig. 3C). Cell proliferation of SH and SH containing LL37 was evaluated through CCK-8 analysis at 1, 3, and 5 days post NDF cell culture. The results indicated a consistent increase in the number of cells in each group over the for 5-day period, displaying a proliferation response comparable to the control group, irrespective of the presence of LL37. Additionally, in evaluating the biocompatibility of the composite hydrogel, the survival rate was compared after a 5-day culture. Live/dead staining of cells revealed a significant presence of viable cells, as evidenced by the prominent green fluorescence in the images. These observations suggest that the prepared composite hydrogel exhibits excellent cytocompatibility and is non-toxic (Fig. 3D and Fig. S9D). Additionally, hydrogels that swell can effectively absorb wound exudate and maintain a moist healing environment, which is essential for rapid healing, especially in diabetic wounds that produce exudates with high inflammatory mediators [21]. The equilibrium swelling ratio of the hydrogels correlates positively with glucose levels, showing minimal equilibrium swelling ratio in PBS, whereas equilibrium swelling ratio of the hydrogel was about 15 % in high-glucose conditions, indicating enhanced exudate absorption (Fig. S9E).

Furthermore, LL37 is known to play an important role in the tissue healing process, especially in blood vessel regeneration and cell growth. We performed an in vitro cell migration assay to confirm the involvement of LL37 in cell migration. The NDFs were scratched and cultivated with each hydrogel component. After 24 h of culture, the migration of NDFs increased in the hydrogel containing LL37 (Fig. 4A). We assessed the efficacy of SH@LL37 and various commercial products in promoting wound healing and cell migration under both normal and high glucose conditions (Fig. S10). After 24 h of culture, there was a significant increase in the migration of NDFs when treated with SH@LL37 compared to commercial products. LL37, an antimicrobial peptide, is renowned for its role in stimulating regeneration and its antibacterial properties. It

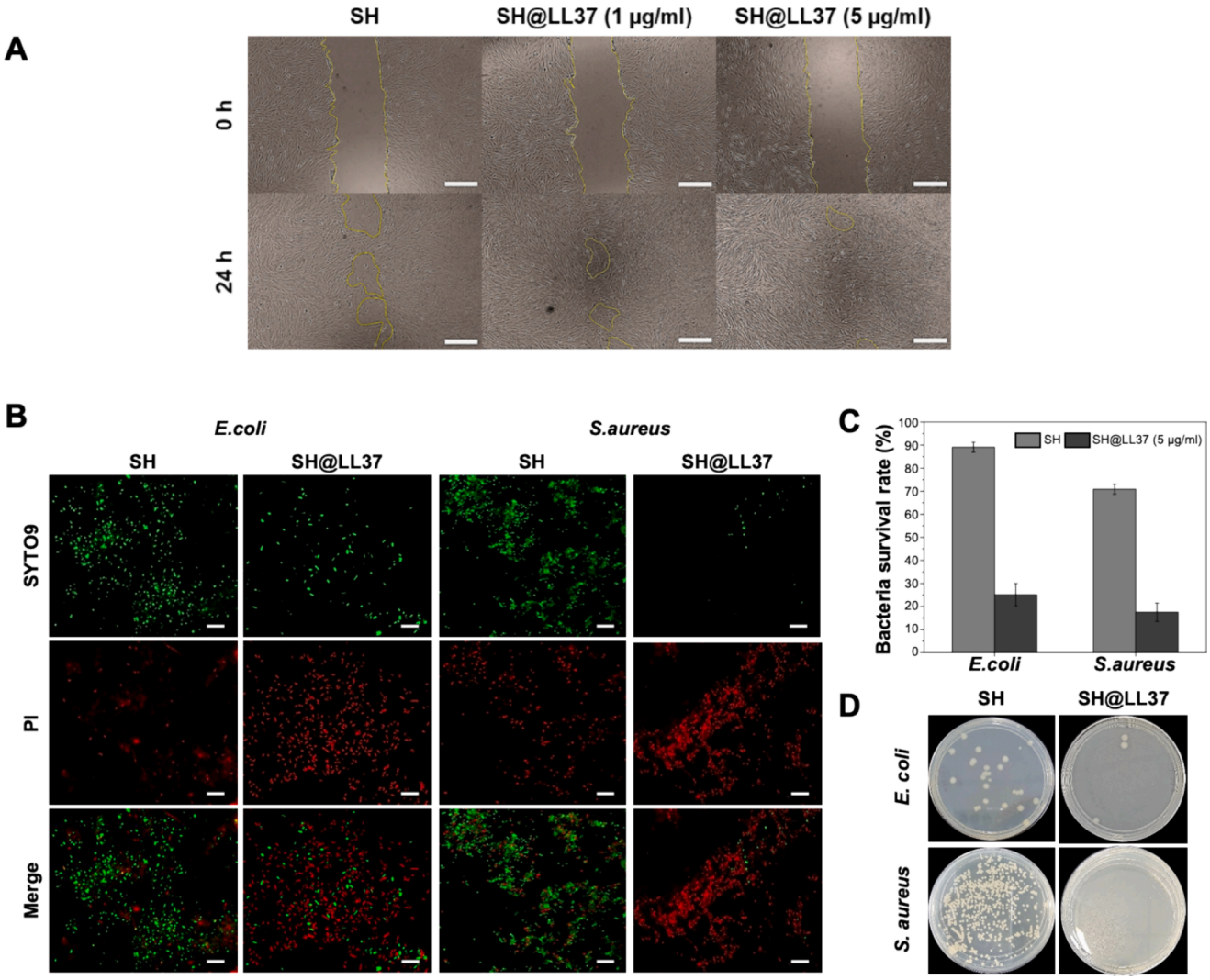

Fig. 4. *In vitro* test of LL37-incorporated sprayable hydrogel. (A) Scratch assay images at different time points (0 and 24 h) of SH@LL37 with varying LL37 concentrations (1 μg/mL and 5 μg/mL) compared to those of SH. Scale bar = 500 μm. (B) Antibacterial activity of sprayable hydrogel (SH) containing LL37 antibacterial peptide compared to SH. Representative live/dead images of *E.coli* and *S. aureus* after contact with the hydrogel. SYTO9 stains surviving cells (green), while propidium iodide (PI) stains dead bacterial cells (red). Scale bar = 10 μm. (C) Quantification of the bacterial survival rate based on the ratio of green to red colored bacteria. (D) Photographs of *E. coli* and *S. aureus* colonies treated with SH and SH@LL37.

exhibits broad-spectrum antibacterial activity against both Gram-positive and Gram-negative bacteria, including *Escherichia coli* (*E.coli*) and *Staphylococcus aureus* (*S. aureus*) pathogens [33,54]. To assess the antibacterial activity of the hydrogel containing LL37, the antibacterial activity against *E. coli* and *S. aureus* was evaluated using the live/dead bacterial viability kit (Fig. 4B). The results showed that SH mainly displayed green fluorescence for both *E. coli* and *S. aureus*, indicating that most of the bacterial cells were alive. In contrast, the composite hydrogel SH@LL37 showed predominantly red fluorescence, indicating that most of the bacterial cells were dead, with approximately 75 % of *E. coli* and about 72 % of *S. aureus* being eradicated. These findings demonstrated the antibacterial activity of the composite hydrogel via LL37, making it a promising treatment for diabetic wounds.

Evaluating and Monitoring Wound Healing in Normal and Diabetic (Hyperglycemic) Animal Models We confirmed that NFs can reveal target genes under both normal and high glucose conditions. Next, we determined whether the NFs would perform similarly *in vivo* using portable fluorescence imaging devices. Each NF (GAPDH-Cy5, PECAM1-Cy3, and COL1A1-Cy3) was first mixed with the hydrogel or PBS and then topically applied to the wounds 4 h after wound creation in mice.

Fig. 5A shows a schematic diagram of the *in vivo* experiment. Blood glucose levels were measured weekly and streptozotocin (STZ) injection was injected at week 2. Mice with blood glucose levels above 250 mg/dL were considered diabetic and used for the *in vivo* experiment [55]. Compared to normal mice (143.98 ± 15.06 mg/dL), diabetic mice (320 ± 41.96 mg/dL) showed continuously elevated blood glucose level after 3 weeks of STZ treatment (Fig. S11A). The experiment was performed for 10 consecutive days and *in vivo* fluorescence imaging was conducted using portable fluorescence imaging devices (100 mm from the wound site, Cy3 = 550–570 nm, Cy5 = 650–670 nm) and subsequently performed for 6 days (on Days 1, 2, 4, 7, and 10).

Fig. 5B shows the remaining wound area (expressed as a percentage) following the application of samples (PBS or hydrogel containing NFs and LL37) in normal and diabetic mice. On day 10 of the experiment, there was a significant difference ($p < 0.0001$) in the remaining wound area between the PBS-treated- and hydrogel-treated groups in both normal and diabetic mice. Compared to the PBS-treated normal mice group (30.01 %), the hydrogel-treated normal mice group showed a decrease in the wound area (16.25 %), and the diabetic group showed a decrease in wound area compared to the PBS-treated diabetic group (32.76 %), respectively.

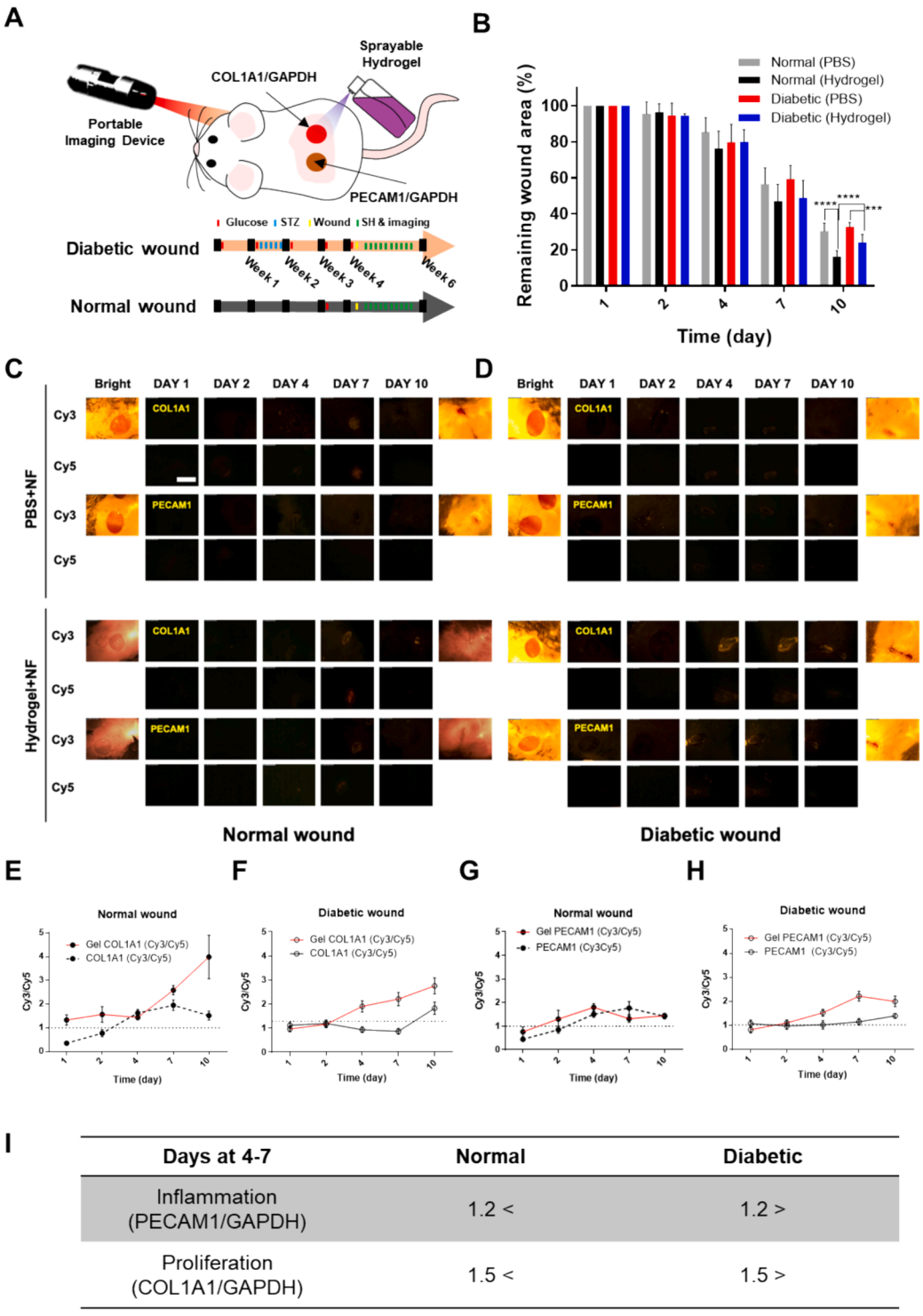

I

Days at 4-7	Normal	Diabetic
Inflammation (PECAM1/GAPDH)	1.2 <	1.2 >
Proliferation (COL1A1/GAPDH)	1.5 <	1.5 >

Fig. 5. *In vivo* application of the LL37 and NanoFlare (NF)-incorporated sprayable hydrogel (SH) to normal and diabetic mice models. (A) Experimental setup of the *in vivo* study (all NFs and SH were topically applied). (B) Remaining wound area (percentage) over time in normal and diabetic wounds. (C) Portable fluorescence imaging of normal mice post NF application on Days 1, 2, 4, 7, and 10. (D) Portable fluorescence imaging of diabetic mice post NF application on Days 1, 2, 4, 7, and 10. (E) Mean fluorescence intensities of COL1A1-NF (*COL1A1/GAPDH*) over time in normal groups, (F) and in diabetic groups. (G) Mean fluorescence intensities of platelet and endothelial cell adhesion molecule 1 (PECAM1)-NF (*PECAM1/GAPDH*) over time in normal groups, (H) and in diabetic groups. (I) Wound Healing Index (WHI). Scale bar = 5 mm.

In addition, normal mice (16.25 %) showed a greater decrease in wound size (−8.02 %p) than diabetic mice (24.27 %) with treatment of hydrogel. Moreover, the hydrogel containing LL37 promoted re-epithelialization and angiogenesis, and improved collagen alignment and deposition (Fig. S12A and S12B).

Fig. 5C-H show quantified fluorescence signals in normal and diabetic mice over time. NF fluorescence signals were quantified using the ImageJ software. By subtracting the background signal from the fluorescence signal, the mean fluorescence intensity was calculated. It was then expressed as the Cy3/Cy5 value, which was further normalized

using the GAPDH-NF signal. Fig. 5E-F show the change of *COL1A1* mRNA fluorescence signal between the hydrogel-treated group and PBS-treated group (control group) in normal and diabetic mice. In normal, hydrogel-treated mice (Fig. 5E, red line) the COL1A1-NF signal increased significantly from day 4, while it (Fig. 5E, black line) gently increased and peaked on day 7 in the PBS group. In diabetic hydrogel-treated mice the COL1A1-NF signal (Fig. 5F, red line) slowly and continuously increased from day 4, while it (Fig. 5F, black line) was stationary and started increasing from day 7 in the PBS-only group. We confirmed that hydrogel helped wound healing in both conditions. Fig. 5G, H showed the fluctuation of the PECAM1-NF signal in normal and diabetic mice. In normal mice, the maximum peak of the PECAM1-NF signal (Fig. 5G, red line) appeared on day 4 in the hydrogel-treated group, while it showed on day 7 in the PBS-treated group (Fig. 5G, black line). In diabetic mice, the peak of PECAM1-NF signal of the hydrogel-treated group (Fig. 5H, red line) was detected on day 7, whereas in the PBS-treated group, the signal showed a slope (Fig. 5H, black line), was mild, and the maximum peak was delayed to day 10. In addition, we observed that ulcer-like wounds were formed in the diabetic mice and the PECAM1-NF signal was emitted continuously on day 10 (Fig. S11B).

To furtherly evaluate the effectiveness of SH on larger wounds, we established hyperglycemic (HG) rabbit models (Fig. S13A-E). SH with each NF (GAPDH-Cy5, COL1A1-Cy3, and PECAM1-Cy3) and LL37 was applied on each wound area. Experimental setup diagram of the *in vivo* study was shown in Fig. S13A. The blood glucose level of > 200 mg/dL were considered to be hyperglycemic [56]. All STZ-treated rabbits showed constantly elevated average blood glucose level (227.00 ± 12.51 mg/dL) throughout the experiment, compared to the normal (normoglycemic) rabbits (126.63 ± 13.86 mg/dL) (Fig. S13B). Graphics of body weight change are shown in Fig. S13C. The photographs of remaining wound area throughout the experiment are shown in Fig. S13D. Fig. S13E shows the remaining wound area (expressed as a percentage) in normal and HG rabbits. On the Day 10 of the experiment, the remaining wound area of hydrogel-treated normal wounds (15.48 %) was smaller than PBS-treated normal wounds (38.18 %). Consistently, in HG wounds, hydrogel-treated HG wounds (16.35 %) showed the smaller remaining wound area than PBS-treated HG wounds (35.62 %).

In summary, in animal models, we confirmed that application of SH promoted wound closure, both in normal and hyperglycemic conditions. Diabetic mice groups exhibited a delay in the signal from NF, and the hydrogel-treated groups displayed a faster maximal fluorescent signal in 2–3 days. This confirmed a decrease in PECAM1 and collagen expression under diabetic conditions, suggesting a potential therapeutic benefit of applying the hydrogel for diabetic wound healing. We also found that application of SH promoted wound closure in rabbits. The findings of this study are consistent with those of previous studies. For example, Eshaq *et al.* reported that there was a loss of PECAM1 in the diabetic retina and plasma in a rat model [57], and Spanheimer *et al.* showed that collagen I production was decreased in a diabetic rat model [58].

Wound Healing Index (WHI) Based on the fluorescence peaks and patterns of each NF signal from Fig. 5E-H, we established the Wound Healing Index (WHI), which served as a reference point for the wound healing status (Fig. 5I). The WHI represents the deviation of diabetic wounds from normal wounds and was calculated by comparing the maximum fluorescence signal of each NF in the diabetic group to that of the control group between days 4 and 7. The WHI for the inflammation (*PECAM1/GAPDH*) stage in normal wounds was defined as greater than 1.2 and less than 1.2 in diabetic wounds. The WHI for proliferation (*COL1A1/GAPDH*) was defined as greater than 1.5 in normal wounds and less than 1.5 in diabetic wounds. When *PECAM1/GAPDH* was less than 1.2, and *COL1A1/GAPDH* was less than 1.5, this indicated delayed wound closure time, decreased matrix deposition, and impaired inflammatory responses. These WHI values can be used to predict the wound healing stage during the inflammatory and proliferative phases, based on molecular biomarker quantification.

In diabetic wounds, the infiltration of immune cells is reduced owing to decreased chemokine and growth factor secretion, which impairs angiogenesis [59]. Additionally, due to the reduced recruitment of immune cells and impaired management of the inflammatory response, “immune senescence” occurs in diabetic wounds [60]. Furthermore, diabetic wounds show reduced transcription of the *COL1A1* gene and altered collagen deposition [61]. In this study, we used *PECAM1* mRNA as an inflammatory biomarker and *COL1A1* mRNA as a proliferative biomarker, as revealed by the NF signal changes. According to the previous study [62], the transition from the inflammatory stage to the proliferative stage is a pivotal step in wound healing. Given that the inflammatory stage is the rate-limiting step in chronic wound [62], our study aimed to establish specific biomarkers for both the inflammatory and proliferative stages, among the overall wound healing process. The objective was to observe and predict the prognosis and trends of diabetic wound healing at a molecular level. In this investigation, the NF signals of two mRNA biomarkers were observed to be delayed and consistently low in diabetic wounds, aligning with findings from previous studies [59–61]. Additionally, from a clinical perspective, the multifunctional SH can be administered to patients in a noninvasive and straightforward manner in the clinical field, and the WHI can be used to predict the condition and prognosis of diabetic wounds as well as the decision of appropriate treatment by medical specialists. In addition, the fluorescence signal of COL1A1-NF is lower than that of the WHI, indicating that there is a lack of *COL1A1* mRNA expression, leading to less collagen deposition in the wound bed [61], with the next step being collagen dressing or skin grafting [63–65]. When PECAM1-NF shows a lower WHI without any inflammation, indicating an impaired immune response at the wound site, extracorporeal shock wave therapy (ESWT) may be used to enhance vascularization and propagate immune responses [27,66].

This study has several limitations. First, although we selected appropriate mRNA biomarkers for various types of cells involved in wound healing, these biomarkers may not fully represent the entire complex process of wound healing *in vivo* because numerous growth factors, proteins, and cells are involved in this process [67–69]. Second, the etiology and condition of chronic wounds, including diabetic wounds, can be diverse [70], and the outcome of treatment with a multifunctional SH on the wound may vary among individuals. Finally, we measured and quantified fluorescence signals in both normal and HG rabbit models (data not shown). Regrettably, the white coat of New Zealand white (NZW) rabbits led to the reflection of NF signal, creating a high background signal. This, in turn, impeded the accurate quantitative expression of the fluorescent signal. Nonetheless, the three mRNA biomarkers (*PECAM1*, *COL1A1*, and *GAPDH*) established in this study were adequately representative of each wound healing process. In addition, as the visualization of mRNA expression by NF was successfully performed using a portable IVIS at the wound site, the application of a multifunctional SH is expected to be a promising technique for monitoring wound healing.

In summary, this wound healing monitoring system enables the real-time assessment of mRNA biomarker expression through fluorescent signals in both normal and diabetic wounds, highlighting the accelerated wound healing rate, active inflammation, angiogenesis, and collagen production facilitated by the applied multifunctional SH.

3. Conclusions

The aim of this study was to develop a user-friendly multifunctional SH that promotes wound healing while monitoring the diabetic wound status. We successfully incorporated LL37 and NFs into the hydrogels, preserved their gelation and spraying properties, and examined their therapeutic effects. The efficacy of LL37- and NF-incorporated hydrogels in promoting wound healing and wound assessment was evaluated in vitro and *in vivo*. Furthermore, we introduced a WHI that provides information on the diabetic wound environment and its changes, aiding

clinicians in making informed decisions regarding wound care. This index serves as a valuable tool for the precise evaluation of the wound healing progress and for optimizing treatment plans for individual patients. Overall, our study demonstrates the potential of SHs for promoting diabetic wound healing and monitoring diabetic wound status, which could have significant clinical applications in the future.

4. Materials and methods

Synthesis of Sprayable Hydrogels. SHs were prepared by mixing the laponite solution with the PAA solution, which was adjusted to pH 7.0 at a concentration of 5 w/w% by adding NaOH solution. First, 200 mg of laponite powder was dissolved in 10 mL of deionized water via magnetic stirring (or vortexing) to prepare a transparent laponite solution. Then, a SH was prepared by adding the specified amount (25, 50, or 100 μL) of the PAA solution and the specified amount (25 or 50 μL) of 10X PBS buffer to 2 mL of the prepared laponite solution. Laponite RD was obtained from BYK (Wesel, Germany). PAA with molecular weights of 5, 100, and 240 k and NaOH were purchased from Sigma-Aldrich (St. Louis, MO, USA).

Cell Culture. THP-1 cells, human monocyte cell line, and RAW 264.7 cells, mouse macrophage cell lines were obtained from the Korean Cell Line Bank (Seoul, Republic of Korea). NDFs were obtained from Promocell (Heidelberg, Germany). NDFs were maintained in Dulbecco's Modified Eagle's medium (DMEM, Sigma-Aldrich). THP-1 cells were maintained in RPMI 1640 (Roswell Park Memorial Institute 1640, Gibco, Billings, MT, USA). RAW 264.7 cells were maintained in DMEM (Sigma-Aldrich) with 2 mM glutamine (Gibco). All media were supplemented with 10 % heat-inactivated fetal bovine serum (Gibco), and 1 % penicillin/streptomycin (Hyclone, Logan, UT, USA) in a 37 °C, 5 % CO_2 atmosphere.

Design and Synthesis of NFs. A modified salt-aging process was used to synthesize NFs according to previous protocols [27]. Fig. S3G show thiol-modified recognition sequences (abbreviated as R) and a flare sequences (abbreviated as F) with a fluorescent dye at the 5′ end. The recognition sequences complemented the target sequence (abbreviated as T). To optimize the sensitivity and stability of the NFs, we adjusted the predicted free energy change of all R-F duplexes to 20 kcal/mol and that of the recognition-target (R-T) to 60 kcal/mol (Fig. S3E). The recognition strand (30 μL, 100 μM) and the flare strand (10 μL, 100 μM) were annealed from 95 °C in a ratio of 3:1 (v/v). Before purification using Micro Bio-Spin 6 columns (Bio-rad, Hercules, CA, USA), the resulting R-F duplex was treated for an hour at 25 °C with 50 mM tris(2-carboxyethyl)phosphine (TCEP) to activate the thiol-modified recognition strand. The purified R-T duplex was mixed with 1 mL of 15 nm citrate-capped GNPs (5 nM, Bioneer, Daejeon, Republic of Korea). After storing the mixture at −20 °C for 2 h, 50 μL of 1 M NaCl was added every 30 min until the final NaCl concentration reached 0.3 M [71]. The solution was sonicated for 30 s after each NaCl addition. After overnight incubation, the functionalized NFs were obtained by centrifugation at 14,000 × *g* for 30 min. The NFs were washed twice with 0.05 % Tween-20-containing PBS. The concentrations of the NFs were determined by measuring the absorbance at 520 nm (Nanodrop 2000, Thermo Fisher Scientific, Waltham, MA, USA). A dynamic light scattering system (Zetasizer Pro, Malvern Panalytical, Malvern, UK) was used to assess the hydrodynamic size and zeta potential of spherical nucleic acids (SNAs) (Fig. S4A-B). The R-F nucleotide sequences of COL1A1-, PECAM1-, and GAPDH-NFs are presented in Fig. S3G.

Hybridization of NFs with Target Nucleotides. 50 μL of NFs at the final optical density (OD) of 0.4 were mixed with target nucleotides for 10 min in the 96-well black plates. The fluorescence intensities were measured at 570 nm (Cy3) for COL1A1-, PECAM1-NF, and 670 nm (Cy5) for GAPDH-NF with SpectraMax i3 Microplate Reader System (Molecular Devices, San Jose, CA, USA). To test the sensitivity of NFs, target nucleotide concentrations were varied from 0 to 10 μM. The fold change of the fluorescence signal was measured by mixing the target or wrong target nucleotides (2 μM) with each NF. All measurements were performed identically three times in duplicate.

Quantification of Target Genes using NFs. Cells in 24-well plates were starved for 24 h in DMEM with 1 % fetal bovine serum (FBS). Five exogenous growth factors (TNF-α, TGF-β1, IL-6, PDGF, and FGF-2) were treated independently to the medium for NDF, THP-1, and M2-like macrophages, respectively. After 2 days, cells were washed with PBS and treated with 5 % FBS medium containing NFs (final OD of 0.1). After 16 h, the cells were stained with Hoechst 33,342 (Invitrogen, Waltham, MA, USA) and subjected to laser scanning confocal fluorescence microscopy (LSM 800; Carl Zeiss, Jena, Germany).

qPCR Analysis for the Selection of Target Sequences. Primers used for the qPCR analysis of *COL1A1*, *PECAM1*, and *GAPDH* mRNAs are presented in Fig. S3F. Cells were seeded into 6-well plates at a density of 2.0×10^4 cells/well without stimulation and cultured to reach 80 % confluency. Then, TNF-α (40 ng/mL), TGF-β1 (40 ng/mL), IL-6 (40 ng/mL), PDGF (20 ng/mL), FGF-2 (40 ng/mL), and NFs were added to an OD of 0.1, for 48 h. A second set of experiments was performed using the same growth factors and 25 mM glucose. Cells were harvested for total RNA extraction using an RNA Extraction Kit (Bioneer, Daejeon, Republic of Korea). One microgram of RNA was reverse transcribed using the cDNA Master Mix (CellScript™, CellSafe, Yongin, Republic of Korea), and qPCR analysis was performed using the QuantStudio 3 Real-Time PCR Detection System (Thermo Fisher Scientific). Primers were purchased from Bioneer. Expression levels of *COL1A1* and *PECAM1* mRNAs were normalized to *GAPDH* mRNA expression using the delta-delta Ct ($2^{-\Delta\Delta Ct}$) method. Each experiment was performed in triplicate. For the growth factor stimulation, cells were first starved for 24 h in DMEM with 1 % FBS before the addition of growth factors for one day.

Polarization of THP-1 Cells into M2 Macrophages. THP-1 cells were seeded in a 24-well plate at a density of 2.0×10^4 cells/well without stimulation and maintained in RPMI 1640 medium supplemented with heat-inactivated 10 % FBS and 1 % antibiotics (penicillin–streptomycin) solution. Polarization into M2 macrophages was induced by exogenous treatment with 40 ng/mL each of IL-4 and IL-10 for 7 days. The experimental groups were as follows: (1) no treatment group, (2) high glucose (25 mM)-treated group, (3) IL-4- and IL-10-induced polarization into M2 macrophages, and (4) IL-4- and IL-10-induced polarization under high glucose (25 mM) conditions. Polarization of M2 macrophages was observed by immunocytochemical staining for the M2 macrophage marker, CD206. CD206 was stained with green fluorescence (FITC) and the nuclei were counterstained with diamidino-2-phenylindole (DAPI). Visualization was performed using an LSCM (LSM 800; Carl Zeiss). Total fluorescence was measured and analyzed using ImageJ software.

Monitoring Mouse PECAM1 Signals in Inflammatory Conditions. RAW 264.7 macrophages were seeded in 6-well-plates with 70 % of confluency. The next day, TNF-α (40 ng/mL), IL-6 (40 ng/mL), and lipopolysaccharide (LPS, 100 ng/mL), were added in the wells. Subsequently, PECAM1-NF: OD 0.1 was added and incubated for 16 h. LSCM (LSM 800, Carl Zeiss) images were obtained at 520–570 nm.

Preparation of NF- and LL37-incorporated Hydrogel. The previously prepared laponite solution (1 mL) and PAA solution (25 μL) were mixed with 25 μL of 10X PBS buffer, 50 μL of NF, and 1 mg/mL concentration of LL37 5 μL, and vortexed to finally produce an SH containing a nanosensor and a regeneration accelerator.

***In vitro* LL37 Release Test.** A 500 μL sample of hydrogel was prepared in a centrifuge tube. Then, 5 mL of PBS was added to the tube, which was subsequently placed in a shaker incubator set to 37 ℃ and 150 rpm. Following the designated incubation time, 1 mL of the supernatant was extracted for analysis. To maintain a consistent volume, 1 mL of fresh PBS was added to the tube [22]. The concentration of LL37 released from the hydrogel was determined using a double-sandwich ELISA in accordance with Hycult Biotechnology's protocols.

Swelling Ratio of Hydrogels. For the equilibrium swelling ratio test, the hydrogels with the same volume were put into PBS and glucose

solution until swelling equilibrium, following by taken out the samples and then weighed after the removal of superfluous water. The equilibrium swelling ratio was calculated as: Equilibrium swelling ratio (%) = $(W_s\text{-}W_d)/W_d \times 100$ %, where W_s and W_d represent the weight of the hydrogels at the swollen and initial weight, respectively [21].

Characterization of Mechanical Properties of Hydrogels. The storage modulus (G') and loss modulus (G') of the hydrogels were measured using a rheometer (Anton Parr, AT) equipped with a steel plate of 25 mm. In all tests, the gap between the plate and the sample platform was set at 0.5 mm at 25 °C, and the modulus was measured as a function of angular frequency under the condition of 1 % strain. For the recovery test, the strain frequency was fixed at 6.3 rad/s, 500 % strain was applied for 2 min, and 0.5 % strain for 3 min to confirm recovery elasticity.

***In vitro* Biocompatibility and Wound Closure Test.** NDFs were purchased from KORAM BIOTECH CORP (Seoul, Republic of Korea) and cultured in DMEM supplemented with 10 % FBS (Welgene, Daegu, Republic of Korea) and 1 % penicillin/streptomycin (Gibco) at 37 °C and in the presence of humidified 5 % CO_2. Cytotoxicity and proliferation evaluation were measured using the CCK-8 assay kit (Dojindo Laboratories, Kumamoto, Japan). NDFs were incubated in 24-well plates at a density of 1 x 10^4 cells/well, induced growth to 70 to 80 % confluence, and then incubated with hydrogel for 1, 3 and 5 days. After washing the plate three times with Dulbecco's Phosphate Buffered Saline (DPBS), NDFs were incubated for 4 h at 37 ℃ using fresh medium and CCK-8 reagent at a 10:1 ratio. Finally, the absorbance of the supernatant was measured at 450 nm using a VersaMax Microplate Reader (Molecular Devices). To evaluate cell viability, after 5 days of culture, cells were stained using the Live/Dead Viability/Cytotoxicity Assay Kit (Thermo Fisher Scientific, Waltham, MA, USA) and observed under a fluorescence microscope. Scratch experiments using NDFs were conducted under the same medium conditions as described above, and seeded on a 12-well plate at a concentration of 1×10^5 cells/well and cultured in DMEM. The medium was then replaced with DPBS and a single scratch was created using a 200 μL pipette tip with the plate bottom fixed vertically. After removing the suspended cells released during scratching by washing the plate twice with Dulbecco's Phosphate Buffered Saline (DPBS), DMEM was added and SH, SH@LL37, BARRICOL, BARRICOL-H, RECELLRO, and NEOSTIN were added to the Transwell (pore size 0.4 μm) insert to observe the migration state of the cells with an optical microscope after 24 h.

Scanning Electron Microscope (SEM) Analysis. Scanning electron microscope (SEM) images were obtained using an FEI Nova Nano SEM 450. For measurement, the hydrogel was freeze-dried for 24 h, and the samples were then sputtered with platinum for 180 s at 2 mA before observation.

***In vitro* Antimicrobial Activity Test.** To test the antibacterial activity, 1 mL each of 1×10^6 CFU/mL Gram-negative (*E. coli*) and 4.8×10^8 CFU/mL Gram-positive (*S. aureus*) bacterial suspensions were dispensed onto Si substrates (1×1 cm^2). The substrates were then placed in a bacterial shaker (50 rpm at 37 °C) and incubated overnight. Following an 18-h incubation, the substrate was carefully washed three times with PBS to remove excess bacteria. Subsequently, 1 mL of hydrogel was dispensed onto each substrate and incubated for 4 h. After the incubation, the hydrogels were removed, washed with PBS, and the bacterial cell viability was assessed using a commercial LIVE/DEAD® BacLight™ kit (Thermo Fisher Scientific), following the manufacturer's instructions. The fluorescently stained samples were observed using a laser scanning confocal fluorescence microscope (LSM 700; Carl Zeiss). In addition, a 1 mL aliquot of *E. coli* suspension (1×10^8 CFU/mL) and *S. aureus* suspension (4.8×10^8 CFU/mL) was added on to the hydrogel and incubated for 24 h at 37 ℃. The incubated cell suspensions were then harvested, serially diluted, and spread onto Lysogency broth (LB) agar plates to assess colony viability.

Experimental Animals. To evaluate the self-healing property of the hydrogel, the Institutional Animal Care and Use Committee (IACUC) of KIST authorized all animal treatments and experimental procedures (Protocol No. KIST-IACUC-2022–014–2). Seven-week-old SD male rats (DBL, Eumseong, Republic of Korea) were purchased and cared for under specific pathogen-free conditions. The self-healing property of the hydrogel was confirmed by inducing a full-thickness wound model. For the *in vivo* evaluation of the NFs and LL37-incorporated hydrogel, the study protocols were approved by the IACUC of Korea University College of Medicine (Protocol No. KOREA-2022–0102 for mice and KOREA-2023–0093 for rabbits). All techniques used in the animal study were designed and performed to minimize animal suffering. Four-week-old male C57BL/6 mice (Orient Bio Inc., Seongnam, Republic of Korea) and 12-week-old male New Zealand white (NZW) rabbits (DooYeol Biotech, Seoul, Republic of Korea) were used in this study. All mice and rabbits were maintained in a standardized environment with a 12-h/12-h light/dark cycle at 18–25 °C in a semi-specific pathogen-free (SPF) environment at Laboratory Animal Research Center of Korea University College of Medicine. Four groups of mice were randomly assigned as follows: (1) normal (non-diabetic) mice treated with PBS, (2) normal mice treated with the hydrogel, (3) diabetic mice treated with PBS, and (4) diabetic mice treated with the hydrogel. Four groups of rabbits were randomly assigned as follows: (1) normal (normoglycemic) rabbits treated with PBS, (2) normal rabbits treated with the hydrogel, (3) hyperglycemic (HG) rabbits treated with PBS, and (4) HG rabbits treated with the hydrogel.

Establishment of Diabetic Mouse Model. To induce diabetes in mice, 50 mg/kg streptozotocin (STZ) was administered intraperitoneally over 5 days. Before use, STZ was dissolved in 50 mM sodium citrate buffer (pH 5.4). A regular meal and 10 % sucrose water were administered to the mice after putting them back in the cage. On day 6, 10 % sucrose water was replaced with regular tap water. Blood glucose measurements were performed once every 2, 3, or 4 weeks after the STZ injection. Before the blood glucose measurements, all mice underwent a 6 h fast and were anesthetized with 2 % isoflurane (CAS #. 26675–46–7; Troikaa, Ahmedabad, India) diluted in 2 L/min of O_2. A puncture needle was used to collect blood from the caudate vein, and a glucometer (GlucoCare, GC BioPharma, Yongin, Republic of Korea) was used to measure blood glucose levels. In mice, diabetes was considered to induced if the basal blood glucose level was $>$ 250 mg/dL [55].

Establishment of HG Rabbit Model. To induce hyperglycemia in rabbits, a dose of 65 mg/kg STZ was administered intravenously through a venous catheter to auricular vein. A regular meal and 10 % sucrose water were administered to the rabbits after putting them back in the cage for 72 h. After 72 h, blood was collected with 1 ml syringe with 24 G needle (Korea Vaccine, Seoul, Republic of Korea), and blood glucose level was measured using a glucometer (GlucoCare). Rabbits with basal blood glucose level of $>$ 200 mg/dL were considered to be hyperglycemic [56,72].

***In vivo* Evaluation of the NF- and LL37-incorporated Hydrogel in Mice.** Before wound creation, male C57BL/6 mice were anesthetized with alfaxalone (30–60 mg/kg, CAS #. 23930–19–0, Careside, Seongnam, Republic of Korea) and xylazine (10 mg/kg; CAS #. 7361–61–7, Bayer, Leverkusen, Germany), and respiratory anesthesia was administered by diluting 2 % isoflurane in 2 L/min O_2. To prevent pain and infection, ketoprofen (5 mg/kg, CAS #. 22071–15–4, UniBioTech, Yesan, Republic of Korea) and enrofloxacin (10 mg/kg, CAS #. 93106–60–6, Bayer) were administered subcutaneously before the surgical procedure. After shaving and sanitizing the dorsal skin of mice 4 weeks after STZ injection, two wounds were created using a 6 mm biopsy punch (KAI Medical, Tokyo, Japan). The skin was carefully removed, exposing the flap and removing all the connective tissue. To eliminate the variability of individual wounds due to their anatomical location, the samples (hydrogels mixed with NFs and LL37, GAPDH-Cy5 assigned to all spots, and PECAM1-Cy3 and COL1A1-Cy3 assigned to each spot) were divided into experimental groups and assigned topically to the two wound spots. The order of topical application was consistent for all subjects. In the control group, the number of wounds and

application of NFs was the same for uniformity of the experiment; however, PBS was used instead of the hydrogel. Each sample was evenly sprayed on the wound spots at a final concentration of OD 1. After applying the sample, the mice were exposed to an infrared heating lamp for 10 min to ensure that they were well absorbed into the wound spots. The samples were repeatedly distributed to each wound on the 2nd, 4th, 7th, and 10th day after the first fluorescence measurement. After applying the sample, the mice under anesthesia were exposed to a heating pad preheated to 37 °C, so that the sample was well absorbed into the wound. The mice were then transferred to portable fluorescence imaging devices (Dino-Lite, Torrance, CA, USA) and the fluorescence emitted from the wounds was measured. At the time of measurement, the field of view (16 cm) covering the entire mouse, distance, height, and optical gain were maintained constant throughout the measurement. The average Cy5 and Cy3 fluorescence intensities in each region of interest were recorded. The wounds healed spontaneously after 10 d. The wound size was measured on the 1st, 2nd, 4th, 7th, and 10th day. On the 2nd, 4th, 7th, and 10th days after wound formation and the first fluorescence measurement, the same process was repeated to acquire fluorescence images. After all the measurements were completed on Day 10 of the experiment, the mice were sacrificed with CO_2 gas, and skin tissues, including the wounded area, were collected for further study.

***In vivo* Evaluation of the NF- and LL37-incorporated Hydrogel in Rabbits.** 12-week-old male NZW rabbits were anesthetized with 5 mg/kg of xylazine (Bayer), and 3 mg/kg of alfaxalone (Careside), and respiratory anesthesia was administered 2 % isoflurane (Troikaa) diluted with 2 L/min O_2. 5 mg/kg ketoprofen (UniBioTech) and 5 mg/kg enrofloxacin (Bayer) were subcutaneously applied to prevent pain and infection before surgical procedure. After shaving and sanitizing the dorsal skin of normal and HG rabbits, sterile surgical scalpels was used to make two independent 10 mm-diameter wounds. All wounds were created uniformly in size and depth. The samples (PBS or hydrogels mixed with NFs and LL37, GAPDH-Cy5 assigned to all spots, and PECAM1-Cy3 and COL1A1-Cy3 assigned to each independent spot) were applied evenly on the wound. The samples were repeatedly applied to each wound on the 2nd, 4th, 7th, and 10th day after the first fluorescence measurement. After applying the sample, the fluorescence signal emitted from the wounds was measured with portable fluorescence imaging devices (Dino-Lite). The field of view (16 cm) covering the entire wounds, distance, height, and optical gain were maintained constant throughout the measurement. The average Cy5 and Cy3 fluorescence signals of each wound site were measured and analyzed on the 2nd, 4th, 7th, and 10th days after wound formation and the first fluorescence measurement. The wound size was measured on the 1st, 2nd, 4th, 7th, and 10th day. After all the measurements were completed on Day 14 of the experiment, the rabbits were sacrificed with 5 mg/kg potassium chloride (CAS #. 7447–40–7, JW Pharmaceutical, Gwacheon, Republic of Korea), and skin tissues, including the wound area, were collected for further study.

Histological Analysis. The mice skin tissue was fixed using 10 % formalin, followed by a sequential dehydration process using sucrose solutions of 10, 20, and 30 %. Subsequently, the tissue was embedded in OCT and incubated overnight at 4 °C, after which it was rapidly frozen using liquid nitrogen. The frozen skin tissue was then sliced into 18 μm thick sections using the MICROM 17 M325 microtome (Thermo Fisher Scientific). Skin sections were stained with hematoxylin and eosin (H&E) and Masson's trichrome (MT) to analyze collagen deposition in re-epithelialized wounds and regenerated skin tissue.

Statistical Analysis. Prism 8 software (GraphPad Software, San Diego, CA, USA) was used for statistical analyses and data plotting. Statistical tests (*t*-test and one-way analysis of variance [ANOVA]) were performed to obtain *p*-value significance. Data are expressed as mean ± standard deviation (SD), percentage of the mean (%), or percentage points (%p) unless otherwise specified. All cell culture experiments were performed with at least two independent replicates. All *in vivo* experiments were performed independently with a minimum of five subjects, which was sufficient for the statistical analysis. Differences between groups were considered statistically significant at $p < 0.05$.

5. Authors' contributions

The manuscript was written through contributions of all authors. All authors have given approval to the final version of the manuscript. ‡These authors contributed equally.

CRediT authorship contribution statement

Daun Jeong: Writing – original draft, Methodology, Investigation. **Se Youn Jang:** Writing – original draft, Methodology, Investigation, Data curation. **Soonjong Roh:** Methodology, Investigation. **Ji Hye Choi:** Formal analysis, Data curation. **I Ji Seo:** Visualization, Investigation. **Jin Hyuck Lee:** Methodology. **Jihoon Kim:** Validation, Supervision. **Ilkeun Kwon:** Validation, Supervision. **Youngmee Jung:** Validation, Supervision, Resources. **Jangsun Hwang:** Supervision, Project administration, Investigation. **Woo Young Jang:** Project administration, Investigation, Funding acquisition. **Jin Yoo:** Writing – review & editing, Supervision.

Declaration of competing interest

The authors declare that they have no known competing financial interests or personal relationships that could have appeared to influence the work reported in this paper.

Data availability

Data will be made available on request.

Acknowledgment

This research was financially supported by a National Research Foundation of Korea (NRF) grant funded by the Korea government (the Ministry of Science and ICT) (RS-2023-00211412, NRF-2022R1A2C2092726, RS-2023-00302145) and National Research Foundation of Korea (NRF) funded by the Ministry of Education (RS-2023-00248221), a KIST intramural grant (2E33151, and 2E3232L), and Korea University Anam Hospital, Seoul, Republic of Korea (Grant No. K2209761, K2305161, K2313001, K2312991, K12300231). We extend our gratitude to Endovision Co., Ltd (Daegu, Republic of Korea) for generously providing clinical wound dressings, namely BARRICOL, BARRICOL-H, RECELLRO, and NEOSTIN.

Appendix A. Supplementary data

Supplementary data to this article can be found online at https://doi.org/10.1016/j.cej.2024.152711.

References

[1] B. Singh, S. Sharma, A. Dhiman, Design of antibiotic containing hydrogel wound dressings: Biomedical properties and histological study of wound healing, Int. J. Pharm. 457 (2013) 82–91.
[2] R. Dong, B. Guo, Smart wound dressings for wound healing, Nano Today 41 (2021).
[3] W. Li, Y. Zheng, W. Pang, P. Lai, Bio-inspired adhesive hydrogel for wound healing, Biomedical Technology 1 (2023) 65–72.
[4] J.J. He, C. McCarthy, G. Camci-Unal, Development of hydrogel-based sprayable wound dressings for second-and third-degree burns, Adv. Nanobiomed Res 1 (2021) 2100004.
[5] H. Chen, R. Cheng, X. Zhao, Y. Zhang, A. Tam, Y. Yan, H. Shen, Y.S. Zhang, J. Qi, Y. Feng, L. Liu, G. Pan, W. Cui, L. Deng, An injectable self-healing coordinative hydrogel with antibacterial and angiogenic properties for diabetic skin wound repair, NPG Asia Mater. 11 (2019).
[6] Y. Liao, L. Xie, J. Ye, T. Chen, T. Huang, L. Shi, M. Yuan, Sprayable hydrogel for biomedical applications, Biomater. Sci. 10 (2022) 2759–2771.

[7] J. Grip, E. Steene, R.E. Engstad, J. Hart, A. Bell, I. Skjaeveland, P. Basnet, N. Skalko-Basnet, A.M. Holsaeter, Development of a novel beta-glucan supplemented hydrogel spray formulation and wound healing efficacy in a db/db diabetic mouse model, Eur. J. Pharm. Biopharm. 169 (2021) 280–291.

[8] J.I. Dawson, R.O. Oreffo, Clay: New opportunities for tissue regeneration and biomaterial design, Adv. Mater. 25 (2013) 4069–4086.

[9] G.U. Ruiz-Esparza, X. Wang, X. Zhang, S. Jimenez-Vazquez, L. Diaz-Gomez, A. M. Lavoie, S. Afewerki, A.A. Fuentes-Baldemar, R. Parra-Saldivar, N. Jiang, N. Annabi, B. Saleh, A.K. Yetisen, A. Sheikhi, T.H. Jozefiak, S.R. Shin, N. Dong, A. Khademhosseini, Nanoengineered shear-thinning hydrogel barrier for preventing postoperative abdominal adhesions, Nano-Micro Lett. 13 (2021) 212.

[10] M. Rodrigues, N. Kosaric, C.A. Bonham, G.C. Gurtner, Wound healing: A cellular perspective, Physiol. Rev. 99 (2019) 665–706.

[11] R. Mata, Y. Yao, W. Cao, J. Ding, T. Zhou, Z. Zhai, C. Gao, The dynamic inflammatory tissue microenvironment: Signality and disease therapy by biomaterials, Research (wash D C) 2021 (2021) 4189516.

[12] X. Fu, J. Wang, D. Qian, L. Xi, L. Chen, Y. Du, W. Cui, Y. Wang, Oxygen atom-concentrating short fibrous sponge regulates cellular respiration for wound healing, Adv. Fiber Mater. 5 (2023) 1773–1787.

[13] W.K. Stadelmann, A.G. Digenis, G.R. Tobin, Physiology and healing dynamics of chronic cutaneous wounds, Am. J. Surg. 176 (1998) 26S–38S.

[14] B. Kong, C. Qi, H. Wang, T. Kong, Z. Liu, Tissue adhesives for wound closure, Smart Med. 2 (2023).

[15] X. Fu, J. Wang, D. Qian, Z. Chen, L. Chen, W. Cui, Y. Wang, Living electrospun short fibrous sponge via engineered nanofat for wound healing, Adv. Fiber Mater. 5 (2022) 979–993.

[16] H.Y. Park, J.H. Kim, M. Jung, C.H. Chung, R. Hasham, C.S. Park, E.H. Choi, A long-standing hyperglycaemic condition impairs skin barrier by accelerating skin ageing process, Exp. Dermatol. 20 (2011) 969–974.

[17] K.C. McCowen, A. Malhotra, B.R. Bistrian, Stress-induced hyperglycemia, Crit. Care Clin. 17 (2001) 107–124.

[18] J.L. Burgess, W.A. Wyant, B. Abdo Abujamra, R.S. Kirsner, I. Jozic, Diabetic wound-healing science, Medicina 57 (2021) 1072.

[19] W.J. Jeffcoate, K.G. Harding, Diabetic foot ulcers, Lancet 361 (2003) 1545–1551.

[20] T. Hirsch, M. Spielmann, B. Zuhaili, T. Koehler, M. Fossum, H.-U. Steinau, F. Yao, L. Steinstraesser, A.B. Onderdonk, E. Eriksson, Enhanced susceptibility to infections in a diabetic wound healing model, BMC Surg. 8 (2008) 1–8.

[21] J. He, Z. Li, J. Wang, T. Li, J. Chen, X. Duan, B. Guo, Photothermal antibacterial antioxidant conductive self-healing hydrogel with nitric oxide release accelerates diabetic wound healing, Compos. B: Eng. 266 (2023).

[22] Y. Liang, M. Li, Y. Yang, L. Qiao, H. Xu, B. Guo, Ph/glucose dual responsive metformin release hydrogel dressings with adhesion and self-healing via dual-dynamic bonding for athletic diabetic foot wound healing, ACS Nano 16 (2022) 3194–3207.

[23] R. Shetty, H. Sreekar, S. Lamba, A.K. Gupta, A novel and accurate technique of photographic wound measurement, Indian, J. Plast. Surg. 45 (2012) 425–429.

[24] C.R. Kruse, K. Nuutila, C.C. Lee, E. Kiwanuka, M. Singh, E.J. Caterson, E. Eriksson, J.A. Sørensen, The external microenvironment of healing skin wounds, Wound Repair Regen. 23 (2015) 456–464.

[25] B. Melai, P. Salvo, N. Calisi, L. Moni, A. Bonini, C. Paoletti, T. Lomonaco, V. Mollica, R. Fuoco, F. Di Francesco, A graphene oxide ph sensor for wound monitoring, 2016 38th Annual International Conference of the IEEE Engineering in Medicine and Biology Society (EMBC), IEEE, 2016, pp. 1898-1901.

[26] H. Luo, B. Gao, Development of smart wearable sensors for life healthcare, Eng. Regen. 2 (2021) 163–170.

[27] J. Hwang, Y. Seo, D. Jeong, X. Ning, C. Wiraja, L. Yang, C.T. Tan, J. Lee, Y. Kim, J. W. Kim, Monitoring wound healing with topically applied optical nanoflare mrna nanosensors, Adv. Sci. 9 (2022) 2104835.

[28] Y. Liang, J. He, B. Guo, Functional hydrogels as wound dressing to enhance wound healing, ACS Nano 15 (2021) 12687–12722.

[29] S. Tavakoli, A.S. Klar, Advanced hydrogels as wound dressings, Biomolecules 10 (2020) 1169.

[30] D.S. Yoon, Y. Lee, H.A. Ryu, Y. Jang, K.M. Lee, Y. Choi, W.J. Choi, M. Lee, K. M. Park, K.D. Park, J.W. Lee, Cell recruiting chemokine-loaded sprayable gelatin hydrogel dressings for diabetic wound healing, Acta Biomater. 38 (2016) 59–68.

[31] H. Cheng, Z. Shi, K. Yue, X. Huang, Y. Xu, C. Gao, Z. Yao, Y.S. Zhang, J. Wang, Sprayable hydrogel dressing accelerates wound healing with combined reactive oxygen species-scavenging and antibacterial abilities, Acta Biomater. 124 (2021) 219–232.

[32] C.F. Anderson, R.W. Chakroun, M.E. Grimmett, C.J. Domalewski, F. Wang, H. Cui, Collagen-binding peptide-enabled supramolecular hydrogel design for improved organ adhesion and sprayable therapeutic delivery, Nano Lett. 22 (2022) 4182–4191.

[33] Z. Liu, X. Yuan, M. Liu, G. Fernandes, Y. Zhang, S. Yang, C.N. Ionita, S. Yang, Antimicrobial peptide combined with bmp2-modified mesenchymal stem cells promotes calvarial repair in an osteolytic model, Mol. Ther. 26 (2018) 199–207.

[34] R. Koczulla, G. Von Degenfeld, C. Kupatt, F. Krötz, S. Zahler, T. Gloe, K. Issbrücker, P. Unterberger, M. Zaiou, C. Lebherz, An angiogenic role for the human peptide antibiotic ll-37/hcap-18, J. Clin. Invest. 111 (2003) 1665–1672.

[35] S. Jelodari, H. Daemi, P. Mohammadi, J. Verdi, J. Ai, M. Azami, Assessment of the efficacy of an ll-37-encapsulated keratin hydrogel for the treatment of full-thickness wounds, ACS Appl. Bio Mater. 6 (2023) 2122–2136.

[36] C. Cui, T. Wu, X. Chen, Y. Liu, Y. Li, Z. Xu, C. Fan, W. Liu, A janus hydrogel wet adhesive for internal tissue repair and anti-postoperative adhesion, Adv. Funct. Mater. 30 (2020).

[37] P.-I. Au, S. Hassan, J. Liu, Y.-K. Leong, Behaviour of laponite® gels: Rheology, ageing, ph effect and phase state in the presence of dispersant, Chem. Eng. Res. Des. 101 (2015) 65–73.

[38] X. Liu, X. Niu, Z. Fu, L. Liu, S. Bai, J. Wang, L. Li, Y. Wang, X. Guo, A facile approach to obtain highly tough and stretchable laponite(r)-based nanocomposite hydrogels, Soft Matter 16 (2020) 8394–8399.

[39] T.B. Becher, C.B. Braga, D.L. Bertuzzi, M.D. Ramos, A. Hassan, F.N. Crespilho, C. Ornelas, The structure-property relationship in laponite(r) materials: From wigner glasses to strong self-healing hydrogels formed by non-covalent interactions, Soft Matter 15 (2019) 1278–1289.

[40] Y. Pang, J. Liu, Z.L. Moussa, J.E. Collins, S. McDonnell, A.M. Hayward, K. Jajoo, R. Langer, G. Traverso, Endoscopically injectable shear-thinning hydrogels facilitating polyp removal, Adv. Sci. 6 (2019) 1901041.

[41] C. Wang, Z. Gong, X. Huang, J. Wang, K. Xia, L. Ying, J. Shu, C. Yu, X. Zhou, F. Li, C. Liang, Q. Chen, An injectable heparin-laponite hydrogel bridge fgf4 for spinal cord injury by stabilizing microtubule and improving mitochondrial function, Theranostics 9 (2019) 7016–7032.

[42] T. De Serres-Bérard, T.B. Becher, C.B. Braga, C. Ornelas, F. Berthod, Neuropeptide substance p released from a nonswellable laponite-based hydrogel enhances wound healing in a tissue-engineered skin in vitro, ACS Appl. Polym. Mater. 2 (2020) 5790–5797.

[43] H. Takeno, Y. Kimura, Molecularweight effects on tensile properties of blend hydrogels composed of clay and polymers, Polymer 85 (2016) 47–54.

[44] H. Takeno, C. Sato, Effects of molecular mass of polymer and composition on the compressive properties of hydrogels composed of laponite and sodium polyacrylate, Appl. Clay Sci. 123 (2016) 141–147.

[45] J.R. Privratsky, D.K. Newman, P.J. Newman, Pecam-1: Conflicts of interest in inflammation, Life Sci. 87 (2010) 69–82.

[46] S. Mascharak, H.E. Talbott, M. Januszyk, M. Griffin, K. Chen, M.F. Davitt, J. Demeter, D. Henn, C.A. Bonham, D.S. Foster, Multi-omic analysis reveals divergent molecular events in scarring and regenerative wound healing, Cell Stem Cell 29 (2022) 315–327, e316.

[47] G.J. Kotwal, S. Chien, Macrophage differentiation in normal and accelerated wound healing, Macrophages: origin, functions and biointervention (2017) 353-364.

[48] A. Viola, F. Munari, R. Sánchez-Rodríguez, T. Scolaro, A. Castegna, The metabolic signature of macrophage responses, Front. Immunol. 10 (2019) 1462.

[49] U. Saqib, S. Sarkar, K. Suk, O. Mohammad, M.S. Baig, R. Savai, Phytochemicals as modulators of m1–m2 macrophages in inflammation, Oncotarget 9 (2018) 17937.

[50] S. Moulik, J. Karmakar, S. Joshi, A. Dube, C. Mandal, M. Chatterjee, Status of il-4 and il-10 driven markers in experimental models of visceral leishmaniasis, Parasite Immunol. 43 (2021) e12783.

[51] A. Brunn, M. Mihelcic, M. Carstov, L. Hummel, F. Geier, A. Schmidt, L. Saupe, O. Utermöhlen, M. Deckert, Il-10, il-4, and stat6 promote an m2 milieu required for termination of p0106–125-induced murine experimental autoimmune neuritis, Am. J. Pathol. 184 (2014) 2627–2640.

[52] Z.-J. Xu, Y. Gu, C.-Z. Wang, Y. Jin, X.-M. Wen, J.-C. Ma, L.-J. Tang, Z.-W. Mao, J. Qian, J. Lin, The m2 macrophage marker cd206: A novel prognostic indicator for acute myeloid leukemia, Oncoimmunology 9 (2020) 1683347.

[53] A.E. Louiselle, S.M. Niemiec, C. Zgheib, K.W. Liechty, Macrophage polarization and diabetic wound healing, Transl. Res. 236 (2021) 109–116.

[54] K.E. Ridyard, J. Overhage, The potential of human peptide ll-37 as an antimicrobial and anti-biofilm agent, Antibiotics (basel) 10 (2021).

[55] S. Yadav, V. Vats, Y. Dhunnoo, J.K. Grover, Hypoglycemic and antihyperglycemic activity of murraya koenigii leaves in diabetic rats, J. Ethnopharmacol. 82 (2002) 111–116.

[56] T. Kida, H. Oku, T. Sugiyama, T. Ikeda, The mechanism and change in the optic nerve head (onh) circulation in rabbits after glucose loading, Curr. Eye Res. 22 (2001) 95–101.

[57] R.S. Eshaq, N.R. Harris, Loss of platelet endothelial cell adhesion molecule-1 (pecam-1) in the diabetic retina: Role of matrix metalloproteinases, Invest. Ophthalmol. vis. Sci. 60 (2019) 748–760.

[58] R.G. Spanheimer, G.E. Umpierrez, V. Stumpf, Decreased collagen production in diabetic rats, Diabetes 37 (1988) 371–376.

[59] O. Ochoa, F.M. Torres, P.K. Shireman, Chemokines and diabetic wound healing, Vascular 15 (2007) 350–355.

[60] K. Geng, X. Ma, Z. Jiang, W. Huang, C. Gao, Y. Pu, L. Luo, Y. Xu, Y. Xu, Innate immunity in diabetic wound healing: Focus on the mastermind hidden in chronic inflammatory, Front. Pharmacol. 12 (2021) 653940.

[61] H.N. Wilkinson, S.E. Upson, K.L. Banyard, R. Knight, K.A. Mace, M.J. Hardman, Reduced iron in diabetic wounds: An oxidative stress-dependent role for steap3 in extracellular matrix deposition and remodeling, J. Invest. Dermatol. 139 (2019) 2368–2377, e2367.

[62] N.X. Landén, D. Li, M. Ståhle, Transition from inflammation to proliferation: A critical step during wound healing, Cell. Mol. Life Sci. 73 (2016) 3861–3885.

[63] L.I. Moura, A.M. Dias, E. Suesca, S. Casadiegos, E.C. Leal, M.R. Fontanilla, L. Carvalho, H.C. de Sousa, E. Carvalho, Neurotensin-loaded collagen dressings reduce inflammation and improve wound healing in diabetic mice, BBA-Mol. Basis. Dis. 2014 (1842) 32–43.

[64] G. Long, D. Liu, X. He, Y. Shen, Y. Zhao, X. Hou, B. Chen, W. OuYang, J. Dai, X. Li, A dual functional collagen scaffold coordinates angiogenesis and inflammation for diabetic wound healing, Biomater. Sci. 8 (2020) 6337–6349.

[65] C. Holmes, J.S. Wrobel, M.P. MacEachern, B.R. Boles, Collagen-based wound dressings for the treatment of diabetes-related foot ulcers: A systematic review, Diabetes Metab. Syndr. Obes.: Targets Ther. (2013) 17–29.

[66] E. Everett, N. Mathioudakis, Update on management of diabetic foot ulcers, Ann. N. Y. Acad. Sci. 1411 (2018) 153–165.
[67] L.M. Morton, T.J. Phillips, Wound healing update, Semin. Cutan. Med. Surg., WB Saunders, 2012, pp. 33-37.
[68] J. Li, J. Chen, R. Kirsner, Pathophysiology of acute wound healing, Clin. Dermatol. 25 (2007) 9–18.
[69] N.T. Bennett, G.S. Schultz, Growth factors and wound healing: Part ii. Role in normal and chronic wound healing, Am. J. Surg. 166 (1993) 74–81.
[70] R. Harries, J. Torkington, K. Harding, Chapter 7 - advances in acellular extracellular matrices (ecm) for wound healing, in: M.Z. Albanna, J.H. Holmes Iv (Eds.), Skin Tissue Engineering and Regenerative Medicine, Academic Press, Boston, 2016, pp. 125–143.
[71] B. Liu, J. Liu, Freezing directed construction of bio/nano interfaces: Reagentless conjugation, denser spherical nucleic acids, and better nanoflares, J. Am. Chem. Soc. 139 (2017) 9471–9474.
[72] I. Ilahi, A. Asghar, S. Ali, M. Khan, N. Khan, Beneficial effects of pentanema vestitum linn. Whole plant on the glucose and other biochemical parameters of alloxan induced diabetic rabbits, Int. Sch. Res. Notices 2012 (2012).